AGU ADVANCING EARTH AND SPACE SCIENCES

JGR Atmospheres

RESEARCH ARTICLE
10.1029/2022JD038433

**Key Points:**

- All simulations of the Weather Research Forecasting model can reasonably capture the spatial distributions of precipitation, 2 m air temperature, and snow-related variables
- The Milbrandt scheme slightly outperforms the other physical parameterization schemes (PPSs) in simulating the magnitudes of the snow-related variables
- None of the PPSs reproduce the characteristics of lake-effect snow well due to their inaccurate temperature and airflow modeling

**Supporting Information:**

Supporting Information may be found in the online version of this article.

**Correspondence to:**

J. Chen,
jiechen@whu.edu.cn

**Citation:**

Lin, Q., Chen, J., Ou, T., Lai, H.-W., Prein, A. F., & Chen, D. (2023). Performance of the WRF model at the convection-permitting scale in simulating snowfall and lake-effect snow over the Tibetan Plateau. *Journal of Geophysical Research: Atmospheres*, *128*, e2022JD038433. https://doi.org/10.1029/2022JD038433

Received 6 JAN 2023
Accepted 27 JUL 2023



# Performance of the WRF Model at the Convection-Permitting Scale in Simulating Snowfall and Lake-Effect Snow Over the Tibetan Plateau

**Qian Lin[1,2], Jie Chen[1,2], Tinghai Ou[3], Hui-Wen Lai[3], Andreas F. Prein[4], and Deliang Chen[3]**

[1]State Key Laboratory of Water Resources Engineering and Management, Wuhan University, Wuhan, China, [2]Hubei Key Laboratory of Water System Science for Sponge City Construction, Wuhan University, Wuhan, China, [3]Department of Earth Sciences, University of Gothenburg, Gothenburg, Sweden, [4]MMM Laboratory, National Center for Atmospheric Research, Boulder, CO, USA

**Abstract** This study investigated the performance of the Weather Research Forecasting (WRF) model at 4-km horizontal grid spacing in simulating precipitation, 2 m air temperature (T2), snowfall, and lake-effect snow (October 4–8, 2018) over the Tibetan Plateau (TP). Multiple simulations with different physical parameterization schemes (PPSs), including two planetary boundary layer schemes (Yonsei University and Mellor–Yamada–Janjic), no cumulus and multi-scale Kain-Fritsch, two land surface models (Noah and Noah-MP), and two microphysics schemes (Thompson and Milbrandt), were conducted and compared. Compared with gauge observations, all PPSs simulate mean daily precipitation with mean relative errors (MREs) of 27.7%–53.6%. Besides, spatial correlation coefficients (SCCs) between simulated and observed mean daily precipitation range from 0.56 to 0.71. For simulations of T2, all PPSs perform similarly well, even though the mean cold biases are up to about 3°C. Meanwhile, all PPSs exhibit acceptable performance in simulating spatial distributions of snow depth, snow cover, and snowfall amount, with SCCs of 0.37–0.65 between simulations and observations. However, the WRF simulations significantly overestimate snow depth (~0.4 cm mean error) and snowfall amount (MREs >372%). The Milbrandt scheme slightly outperforms the other PPSs in simulating snow-related variable magnitudes. Due to their inaccurate temperature and airflow modeling over the lake surface and its surroundings, none of the WRF simulations well reproduce the characteristics that more snow occurs over the lake and downwind area. Overall, this study provides a useful reference for future convection-permitting climate modeling of snow or other extreme events when using the WRF model in the TP and other alpine regions.

**Plain Language Summary** Snow falls frequently in cold seasons, especially in alpine regions. When there is a lake, a very interesting snowfall phenomenon named lake-effect snow may happen, that is, more snow occurred over the lake and downwind areas. However, the lake-effect snow caused by large lakes over the Tibetan Plateau (TP) may induce snow disaster events. Thus, conducting reliable simulations of lake-effect snow events are essential for understanding the mechanism of these particular events over the TP. This study investigated the performance of the numerical model in simulating precipitation, 2 m air temperature (T2), snowfall, and lake-effect snow (October 4–8, 2018) over the TP. The results show that the simulated precipitation and T2 perform reasonably well, although wet and cold biases are observed. However, the investigated numerical model fails to reproduce the characteristics of this event well, which may be due to the inaccurate temperature and airflow modeling over the lake surface and its surroundings. Continued improvement is needed for future modeling. Hence, this study provides some suggestions for future numerical modeling of lake-effect snow or other snow events over the TP and other alpine regions.

## 1. Introduction

The Tibetan Plateau (TP), often called the "Third Pole," is the largest plateau in the world, with an average elevation of 4,000 m above sea level. It is also referred to as the "water tower of Asia" because it is the headwater of several major Asian rivers, providing fresh water for billions of people (Yao et al., 2022). The TP has the largest number of alpine lakes in the world with more than 1,400 lakes greater than 1 km$^2$ (Ma et al., 2009; Zhao et al., 2022). In recent decades, most lakes over the TP have experienced rapid expansion in terms of their size and number due to global warming (Dong et al., 2018; Zhang et al., 2017, 2020). Lakes areas (when not frozen) are characterized by a low albedo, a low surface roughness, and a high specific heat capacity (Bonan, 1995) and have great impacts on the regional climate through land and atmospheric water and heat exchange (Notaro, Holman, et al., 2013; Wu et al., 2019). In addition, these lakes are an effective indicator of climate change due to the limited anthropogenic influence in this region (Zhang et al., 2020). Hence, quantifying the climatic effect of the lakes over the TP is beneficial to improving our understanding of the changes in the regional hydrological cycle and energy budget (Su et al., 2020; Wu et al., 2019; Xu et al., 2016).

The climatic effects of lakes are determined by the intrinsic lake features, local terrains, and background atmospheric circulations (Argent et al., 2015; Subin et al., 2012; Wen et al., 2015). Thus, they exhibit various diurnal and seasonal characteristics in different regions (Su et al., 2020; Vavrus et al., 2013; Williams et al., 2015). For example, the Great Lakes in North America strongly increase precipitation and heavy snowfall in downwind areas in cold seasons, while leading to a slight decrease in precipitation over the lakes in summer (Eichenlaub, 1970; Notaro, Zarrin, et al., 2013; Scott & Huff, 1996). Moreover, the existence of the Great Lakes reduces the amplitude of the diurnal cycle and the annual cycle of the air temperature over the lakes and surrounding areas (Notaro, Holman, et al., 2013). Different from the Great Lakes, Lake Victoria in the tropics causes reduced air temperature and enhanced precipitation throughout the year (Williams et al., 2015). As one of the largest lakes over the TP, Nam Co Lake has also been found to have an evident lake effect, reducing precipitation by 45%–70% over the lake in summer and enhancing precipitation by 60% over the lake and downwind areas in autumn as a result of the cooling and warming effects of the lake in summer and autumn, respectively (Dai, Yao, et al., 2020). In addition, Qinghai Lake over the TP results in a situation similar to that caused by Nam Co Lake (Su et al., 2020).

In particular, lakes over the TP and in many other places produce a phenomenon known as lake-effect snow (Eichenlaub, 1970) in cold seasons. The lake-effect snow usually occurs when below-freezing air passes over a lake's warmer waters (Eichenlaub, 1970; Lavoie, 1972), which is characterized by more snow occurring over the lake and the downwind areas (Kristovich et al., 2003). Differently from ordinary snow, lake-effect snow tends to produce snow continuously for up to 48 hr over a particular area, which is usually not caused by a low-pressure system. It has been demonstrated that large lakes over the TP can increase snowfall in downwind areas, which plays an important role in causing regional snow disaster events (Dai, Chen, et al., 2020; Zhao et al., 2022). Accordingly, a reliable simulation of lake-effect snow is of great importance for understanding the dynamics and mechanism of these particular events over the TP. In fact, ordinary snow falls more frequently over the TP compared with lake-effect snow, especially at high altitudes. As a crucial component of the climate system, snow plays an essential role in shaping the climate and affecting the water cycle over the TP and its surrounding regions (Henderson et al., 2018; Shen et al., 2015; Xiao & Duan, 2016). Therefore, modeling the evolution of a snowfall event is necessary for revealing the land-atmosphere interactions during specific processes.

The Weather Research Forecasting (WRF; Powers et al., 2017; Skamarock & Klemp, 2008) model is a mesoscale numerical weather prediction system, which has been widely used to simulate snowfall and lake-effect snow events over the TP (e.g., Dai et al., 2018; Dai, Chen, et al., 2020; Li et al., 2009; Su et al., 2020). For example, Liu et al. (2019) used the WRF model to simulate a snow event over the TP in March 2017 and concluded that the WRF model could reproduce both the observed values and the spatial pattern of snow depth at the meteorological stations. In addition, Zhao et al. (2022) adopted the WRF model to quantify the impacts of Nam Co Lake and the surrounding terrain on an extreme snow event. Their results showed that Nam Co Lake played the predominant role in the formation of the investigated snow event, and the surrounding mountains amplified the lake effect precipitation/snow in the downwind areas. The WRF model offers various physical parameterization schemes (PPSs) for selection, an appropriate choice of PPSs to describe land-atmosphere interactions is essential for conducting the simulations of snowfall events. However, current studies provide limited evidence about the sensitivity of PPSs in simulating snowfall and lake-effect snow over the TP, especially at the convection-permitting scale.

The ongoing Convection-Permitting Third Pole (CPTP) project (http://rcg.gvc.gu.se/cordex_fps_cptp/), which is a Flagship Pilot Study (FPS) endorsed by the Coordinated Regional Downscaling Experiment of the World Climate Research Program (CORDEX), aims to enhance the understanding of the water cycle and extremes in the TP region. The objective of the first phase of the project is to assess the model's skill in convection-permitting simulations of convection, precipitation, and snowfall over the TP (Prein et al., 2022). Setting up and testing the models for different meteorological cases over the TP can provide insights into model sensitivities and skills in

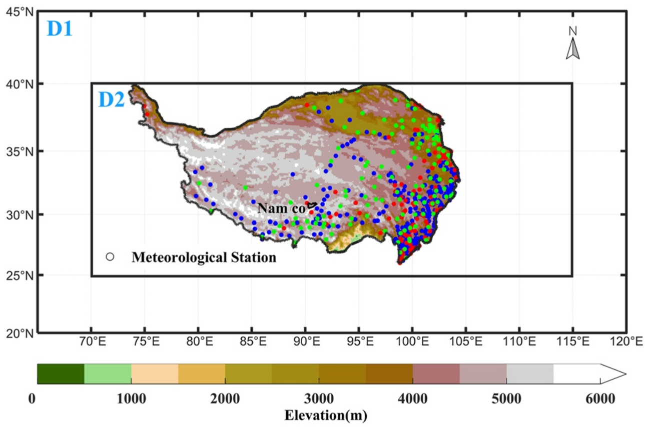


**Figure 1.** Map of the WRF model domain D1 (12 km resolution) and D2 (4 km resolution) used in the CPTP project, and locations of the study area (Tibetan Plateau, China) and the meteorological stations used in the analysis. The blue solid circles denote stations with daily precipitation and temperature gauge data; the red solid circles denote stations with hourly precipitation and temperature gauge data; and the green solid circles denote stations with daily snow depth gauge data.

terms of the representation of certain processes and can guide the modeling strategy for further long-term climate simulations. After an overview of experimental design and model performance in simulating three meteorological cases over the TP in Prein et al. (2022), this study focuses on an in-depth analysis of snowfall and lake-effect snow for the snowfall case simulated by the WRF model. This snowfall event occurred on October 4–8, 2018 (details presented in Section 2.1) over the whole TP, which was accompanied by the occurrence of a typical lake-effect snow event around Nam Co Lake. Specifically, the objective of this study was to evaluate the performance of the WRF model with different PPSs in simulating snowfall and lake-effect snow over the TP based on this snowfall event at the convection-permitting scale. The tested PPSs covered four main types, including two cumulus schemes, two land surface models, two microphysics schemes, and two planetary boundary layer schemes, which will be described in Section 2.2. The remainder of the manuscript is organized as follows. The data and methodology are introduced in Section 2. The results and discussion are presented in Sections 3 and 4, respectively. Finally, the summary and conclusions are presented in Section 5.

## 2. Data and Methodology

### 2.1. Description of the Snowfall Event

The heavy snowfall event (Dai, Chen, et al., 2020) occurred during October 4–8, 2018, around Nam Co Lake (Figure 1). This was the largest snowfall event in October since recording began at Nam Co station in 2005. On 3 October 2018, a gust of cold air passed over the group of lakes, causing the daily minimum temperature in the region to drop by about 4.5°C within 24 hr. As a consequence, the daily minimum temperature reached the freezing point about 1 week earlier than in previous years. During the snow period, the snowfall to the east of Nam Co was more than 50 cm, while it was only 5 cm to the west of Nam Co, with an influence area of about 8,000 km$^2$ (Dai, Chen, et al., 2020), exhibiting typical characteristics of a lake-effect snow event. Meanwhile, extensive snowfall also occurred over the whole TP during this period.

### 2.2. Model Configuration and Experimental Designs

The WRF model is a state-of-the-art atmospheric modeling system designed for meteorological research and numerical weather prediction. The WRF model version 4.2.1 with a turbulent orographic drag scheme (Beljaars et al., 2004; Zhou et al., 2018, 2019) was used in the CPTP project. The forcing data used for the WRF simulations were the fifth generation of the European Centre for Medium-Range Weather Forecasts (ECMWF) atmospheric reanalysis of the global climate (ERA5) (Copernicus Climate Change Service (C3S), 2017), with hourly and $0.25° \times 0.25°$ temporal and spatial resolutions, respectively. Two nested domains with horizontal grid spacings of 12 km (D1) and 4 km (D2) were configured (Figure 1). Only the hourly output in the inner domain (i.e., D2) was utilized in this study. Forty-nine levels were set in the vertical direction. For the WRF simulations, a reference run was used, which was offline nested and initialized from the 12 km grid spacing simulations (performed on D1) and started 18 months before the case occurrence. That is, the 4 km (D2) simulations were initialized using the conditions from about 18 months of the 12 km (D1) spin-up simulations.

The PPSs for the reference run were set as follows: the rapid radiative transfer model for general circulation models (RRTMG) scheme for longwave and shortwave radiation (Iacono et al., 2008), no cumulus parameterization (CU), the Thompson scheme for the microphysics (MP) (Thompson et al., 2008), the Yonsei University (YSU) scheme for the planetary boundary layer (PBL) (Hong et al., 2006), and the Noah-MP (multi-physics) land surface model for the land surface model (LSM) (Niu et al., 2011). These physics settings of the reference run have been proven to perform well in the U.S (Liu et al., 2017). To examine the performances of the different PBL, CU, LSM, and MP schemes in simulating snowfall and lake-effect snow, five different simulations were performed using the WRF model. In addition to the reference run, in the other four simulations, only one of the

10.1029/2022JD038433

**Table 1**
*Summary of Set-Ups Used in All Simulations*

| Sim_id | PBL | CU | LSM | MP |
|---|---|---|---|---|
| Reference-run | YSU | \ | Noah-MP | Thompson |
| PBL-MYJ | **MYJ** | \ | Noah-MP | Thompson |
| CU-MSKF | YSU | **MSKF** | Noah-MP | Thompson |
| LSM-Noah | YSU | \ | **Noah** | Thompson |
| MP-Milbrandt | YSU | \ | Noah-MP | **Milbrandt** |

*Note.* Bold PPSs indicate the PPSs that were changed for each simulation compared with the reference run. PBL, planetary boundary layer; CU, cumulus; LSM, land surface model; MP, microphysics.

PPSs was changed at a time, while all of the other schemes were set identically to the reference run. For the selection of the PPSs, at least one of the following criteria should be satisfied: (a) they are widely used in the WRF community; (b) they have excellent performance according to previous studies; and (c) they are not tested in Prein et al. (2022).

In total, the PPSs of these simulations covered two PBLs, two CUs, two LSMs, and two MPs (Table 1). Then, the four different sets of PPSs were compared as follows: the YSU scheme and Mellor-Yamada-Janjic (MYJ) (Janjic, 1994) scheme, the no-cumulus scheme and multi-scale Kain-Fritsch (MSKF) (Zheng et al., 2016) scheme, Noah-MP LSM and Noah LSM (Tewari et al., 2004), and the Thompson scheme and Milbrandt scheme (Milbrandt & Yau, 2005a, 2005b). Next, a brief description of these PPSs is given. The YSU scheme is a first-order nonlocal scheme, which has been successfully implemented in the WRF model to produce a more realistic structure and development of the PBL (Hong et al., 2006). The MYJ scheme uses the 1.5-order turbulence closure model to represent turbulence above the surface layer (Janjic, 1994), which is suitable for all stable and slightly unstable flows, but a large error is likely to appear in the convective boundary layer. The MSKF scheme introduced scale-aware parameterized cloud dynamics for high-resolution forecasts by modifying based on the Kain-Fritsch convective parameterization scheme (Zheng et al., 2016), which outperforms the other cumulus schemes in simulating precipitation of the TP in terms of both the mean intensity and diurnal cycles with a horizontal resolution of 9 km (Ou et al., 2020). The Noah-MP and Noah LSM are both widely used LSMs in the WRF model, but the Noah-MP LSM is more complex than the Noah LSM with more advanced physical parametrization schemes. The Noah LSM combines vegetation with a bulk layer of snow and soil by using a surface layer, while the Noah-MP LSM uses a separate vegetation canopy layer and three snow layers based on the Noah LSM (Liu et al., 2019). The Thompson scheme contains prognostic equations for cloud water, cloud ice, snow, rain, and graupel mass mixing ratios. To increase the accuracy and maintain computational efficiency, only the cloud ice and rainwater species are double moment in the Thompson scheme (Thompson et al., 2008). The Milbrandt scheme is double moment for all species, with separate classes for graupel and hail (Milbrandt & Yau, 2005a, 2005b), which may have great potential in simulating snowfall events (Milbrandt et al., 2012).

### 2.3. Methodology for Evaluating Model Performances

#### 2.3.1. In-Situ Observations

In-situ observations were used as references to evaluate the performance of the WRF in simulating the precipitation, air temperature at 2 m (T2), and snow depth. These in-situ observations were provided by the Chinese Meteorological Administration (CMA), including daily precipitation and T2 for 529 stations, hourly precipitation and T2 for 126 stations, and daily snow depth data for 125 stations in the study area (i.e., TP) during the study period (i.e., October 4–8, 2018) (Figure 1).

#### 2.3.2. Gridded Observations

Since the meteorological stations were mainly located on the central and eastern TP, a remote sensing-based gridded precipitation product and a station-based gridded temperature data set were also applied as supplements to better investigate the temporal and spatial distributions of the simulated precipitation and T2.

The gridded precipitation was derived from the Global Precipitation Measurement (GPM) Mission. The integrated multi-satellite retrievals for the GPM (IMERG) final run product (Huffman et al., 2019) were used in this study, with a temporal resolution of 30 min and a spatial resolution of 0.1° (~10 km). Although GPM data has been widely used in many studies over the TP (Li, Qi, & Chen, 2022; Lin et al., 2021; Ou et al., 2020), it has a deficiency in terms of detecting snowfall (Behrangi et al., 2014; Immerzeel et al., 2015). Therefore, the GPM precipitation was compared with the gauge observations to confirm if it was suitable for use as a reference at the grid scale from October 4 to 8, 2018, over the TP. When compared with the gauge observations, the GPM precipitation of the closest grid points was used. As can be seen from Figure S1 in Supporting Information S1, the GPM mean daily precipitation data exhibits a spatial distribution similar to that of the gauge station data, with a spatial correlation coefficient (SCC) of 0.73. In addition, the GPM data is slightly drier than the gauge observations

10.1029/2022JD038433

during October 4–8, 2018, with a mean relative error (MRE) of −12.9%. Although the reliable performance of the GPM mean daily precipitation is not found at some gauge stations due to their locations and complex surrounding terrain, GPM generally reproduces the mean daily precipitation of most gauge stations during the study period. Thus, using the GPM data as a reference is still reasonable for evaluating the performance of the WRF model in simulating precipitation at the grid scale.

The gridded temperature data were obtained from the China meteorological forcing data set (CMFD), which was created through a fusion of remote sensing products, reanalysis data sets, and in-situ observations at meteorological stations (He et al., 2020; Yang & He, 2019). The temporal resolution of the CMFD is 3 hr and the spatial resolution is 0.1° (∼10 km). The reasonable performance of this data set in capturing the observed temperature over the TP has been shown in previous studies (Li, Qin, et al., 2022; Xie et al., 2017; Yang et al., 2021).

In addition, to evaluate the performance of the WRF model in simulating the snow-related variables, the probability of liquid precipitation (PL) of the GPM was also used. The PL within the range of 0%–100% was calculated based on the wet-bulb temperature using the method of Sims and Liu (2015), which can be applied to estimate the precipitation phase (rain, sleet, and snow) for any global precipitation field (Huffman et al., 2019). The higher the PL value is, the more likely the precipitation will fall as rain. According to a previous study, if the PL within a half-hour interval is less than 20%, the precipitation during this half-hour can be considered to be snow over the TP (Li, Qi, & Chen, 2022). Thus, 20% was used as the threshold for distinguishing the snow phase to calculate the snowfall amount of the GPM in this study. In addition, a new Medium Resolution Imaging Spectroscopy (MODIS) snow cover extent product over China (Hao, 2021) was also used to assess the performance of the WRF model in simulating the snow cover. This product was produced based on MOD09GA/MYD09GA surface reflectance data and has higher accuracy than standard MODIS snow products (Hao et al., 2022).

#### 2.3.3. Evaluation Metrics

The performances of the WRF model in simulating the precipitation, T2, and snow-related variables were evaluated using three commonly used statistical metrics: the mean error (ME), MRE, and SCC. Among these metrics, the ME was used to calculate the deviation of the T2 and snow depth, which demonstrates the systematic deviation of the simulations from the observations. Considering there are great seasonal and regional variations of precipitation (or snowfall amount) over the TP, the MRE was used to describe the deviation degree of the simulated precipitation (or snowfall amount) from the observations. The MRE was calculated by dividing the precipitation (or snowfall amount) difference between the WRF simulations and the observations (the WRF simulations minus observations) by the observations. The SCC was applied to measure the ability of simulations to reproduce the spatial distributions of precipitation, T2, and snow-related variables. When calculating the statistical metrics based on station observation data, the gridded precipitation, T2, and snow depth from the WRF simulations were interpolated to the locations of the stations using the nearest-neighbor interpolation method, and the gridded observations were re-interpolated to the WRF grids using the bilinear interpolation method.

## 3. Results

All of the WRF simulations were performed for the heavy snowfall event, and thus, the analyses focused on the snow-related variables. Considering precipitation and temperature are the two most important variables for the hydrological cycle, they were also analyzed.

### 3.1. Performance of WRF in Simulating Precipitation

The spatial distributions of the mean daily precipitation averaged from October 4 to 8, 2018, for the GPM, gauge observations, and WRF simulations are shown in Figure 2 and Figure S2 in Supporting Information S1. The results show that the precipitation was mainly concentrated over the southeastern TP during October 4–8, 2018, and the maximum value was >10 mm/d. The spatial distributions of the mean daily precipitation are similar for all of the WRF simulations and agree well with both the gauge observations and GPM, with the SCCs ranging from 0.56 to 0.71. The MRE values of the mean daily precipitation relative to the gauge observations and GPM are presented in Figure S3 in Supporting Information S1. All of the WRF simulations exhibit wet biases for most of the stations and grids over the TP. However, the MRE values of the mean daily precipitation are generally larger when compared with the GPM. This may be because that the GPM is drier than the gauge observations.

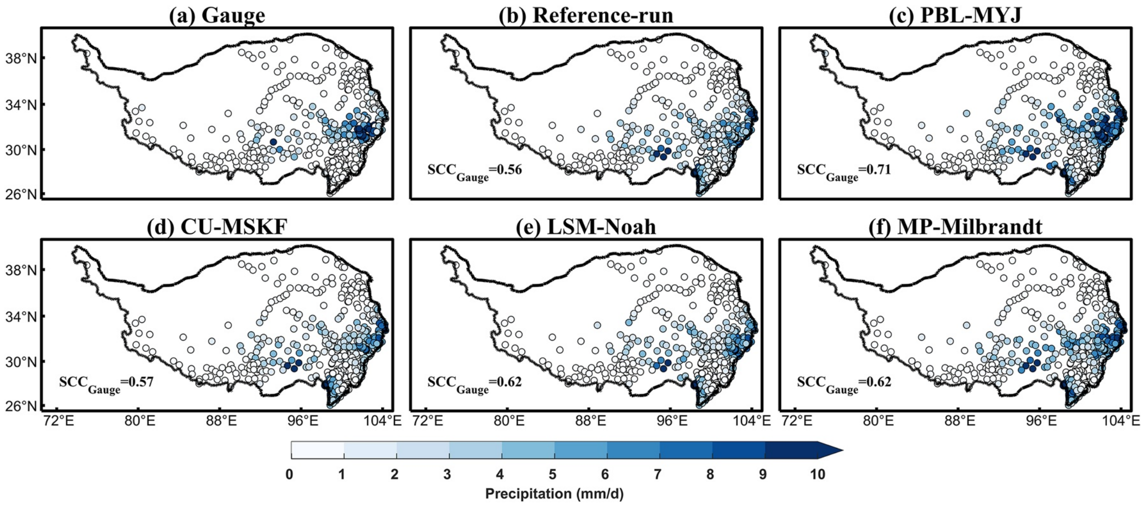


**Figure 2.** Spatial distributions of mean daily precipitation averaged from October 4 to 8, 2018: (a) gauge observations, and (b–f) WRF simulations over the gauge stations, with SCC calculated based on gauge observations.

In addition, the YSU scheme, MSKF scheme, Noah LSM, Thompson scheme respectively show lower MREs than the PPSs of the same type in simulating the mean daily precipitation, with the mean MREs ranging between 27.7% and 53.6% (between 35.6% and 80.2%) compared with the gauge observations (GPM). The accumulated precipitation of the gauge observations, GPM, and all of the WRF simulations during October 4–8, 2018 averaged over 126 stations were also analyzed (Figure 3). Figure 3 also shows that all of the simulations capture the temporal variability of the observed accumulated precipitation, but they exhibit wet biases. Moreover, the accumulated precipitation of the MSKF scheme and Noah LSM is about 11 mm, which is relatively close to the gauge observations. The MYJ scheme has the largest wet bias among all of the WRF simulations, with accumulated precipitation of about 13 mm. According to the previous study, these wet biases are probably caused by the complex terrain in the TP, which produce more precipitation by enhancing the uplift of small and medium-sized terrain in the simulations (Ren et al., 2020).

In summary, the above results demonstrate the general agreement between the WRF simulations and the observations for precipitation. When using the GPM and gauge observations as references, the simulation with the YSU scheme, MSKF scheme, Noah LSM, and Thompson scheme perform better than the other combinations in simulating the precipitation during this snowfall event.

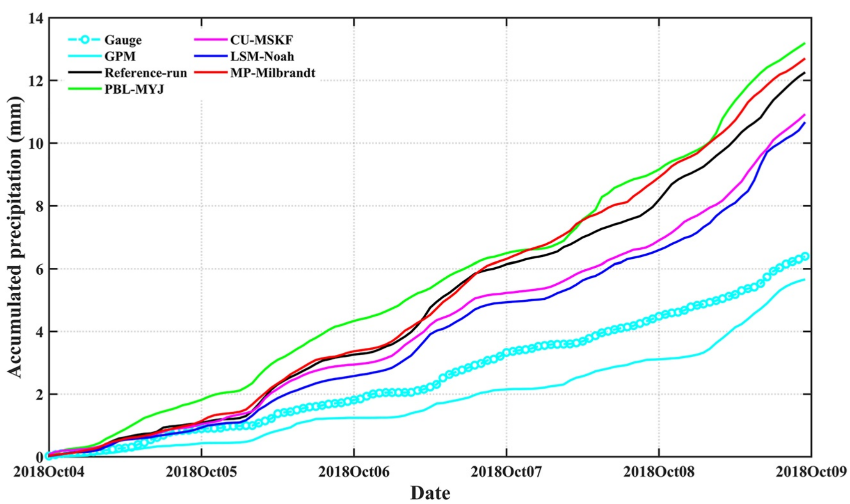


**Figure 3.** Accumulated precipitation for the gauge stations, GPM, and WRF simulations during October 4–8, 2018. The values are averaged over 126 stations.

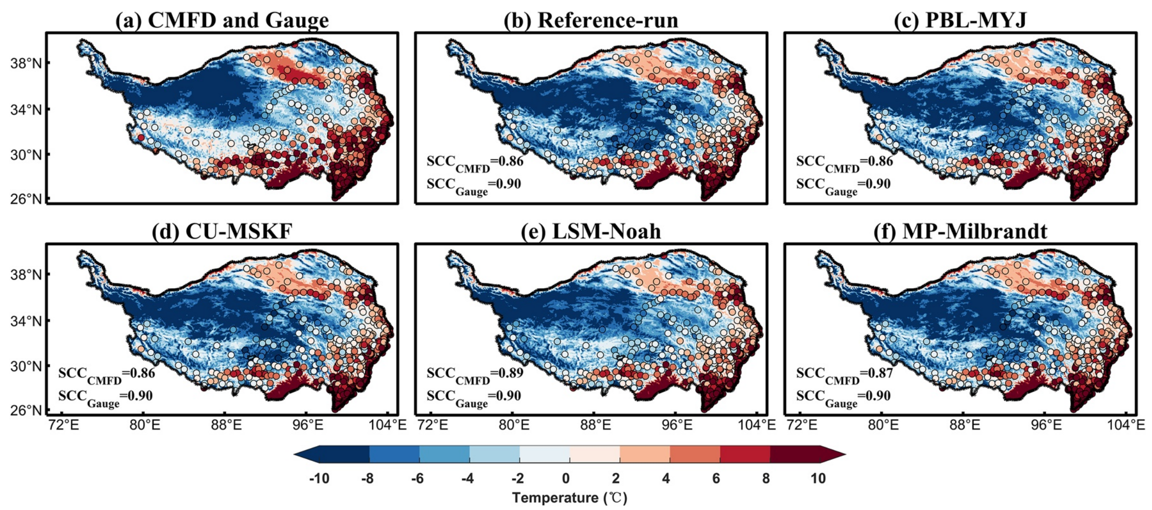


**Figure 4.** Spatial distributions of mean daily T2 averaged from October 4 to 8, 2018: (a) CMFD and gauge observations, and (b–f) WRF simulations over the WRF grid cells and gauge stations, with SCC calculated based on CMFD and gauge observations.

### 3.2. Performance of WRF in Simulating T2

Figure 4 shows the spatial distributions of the mean daily T2 averaged from October 4 to 8, 2018, for the CMFD, gauge observations, and WRF simulations. The mean daily T2 in the southern and northeastern TP was up to 20°C warmer than that in other areas of the TP during October 4–8, 2018. The spatial distributions of the mean daily T2 for all of the WRF simulations agree well with the gauge observations and CMFD, and all of the SCC values are >0.86. The ME values of mean daily T2 relative to the gauge observations and CMFD are shown in Figure S4 in Supporting Information S1. The results show that the WRF simulations exhibit cold biases at both the station and grid scales, which is consistent with the results of previous studies (e.g., Lin et al., 2021; Prein et al., 2022; Wang et al., 2021). In addition, the cold biases relative to the gauge observations are larger than the cold biases relative to the CMFD, with ME values ranging from −5° to 0°C for most of the stations. The mean ME values calculated based on the CMFD range from −2° to −1°C and are generally 1°–2°C smaller than those calculated based on the gauge observations. This may have been because the in-situ stations are mostly located in valleys (Li, 2018).

The performance of the WRF model in simulating the hourly T2 time series during October 4–8, 2018 is displayed in Figure 5. The results show that the variability of the hourly T2 from the CMFD and all of the WRF simulations agree well with that of the gauge observations from October 4 to 8, 2018. Independent of the PPSs, all of the simulations exhibit an overall cold bias relative to the gauge T2 observations, which is probably linked to the well-known systematic cold bias of the WRF model in high altitude areas (Bonekamp et al., 2018; Gao et al., 2015; Lin et al., 2021). The cold biases range from −5° to 0°C, and the maximum values occur at the maximum and minimum T2 on each day. In general, all of the WRF simulations reproduce well the spatiotemporal distribution of T2 over the TP, and their performances in simulating T2 are quite similar.

### 3.3. Performance of WRF in Simulating Snow-Related Variables

#### 3.3.1. Snow Depth and Snow Cover

The snow depth is an important indicator of the intensity of a snow event (Liu et al., 2019), and thus, it was the first snow-related variable analyzed in this study. Because there was no suitable gridded snow depth product, the performance of the WRF model in simulating the snow depth was only evaluated at the site scale using the gauge snow depth data for 125 stations over the TP. The spatial distributions of the mean snow depth averaged from October 4 to 8, 2018 for both the gauge observations and WRF simulations are displayed in Figure 6 and Figure S5 in Supporting Information S1. The results show that the snow cover is mainly concentrated on the southeastern and northwestern TP, with a maximum mean snow depth of up to 5 cm. All of the WRF simulations generally capture the spatial pattern of the mean snow depth, with SCC values ranging from 0.37 to 0.45. In addition, the

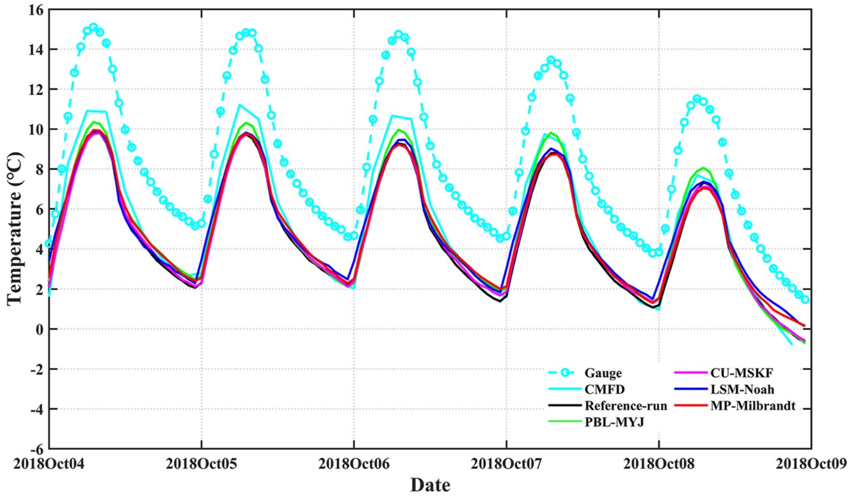


**Figure 5.** Hourly T2 time series for the gauge stations, CMFD, and WRF simulations during October 4–8, 2018. The values are averaged over 126 stations.

MYJ scheme (SCC = 0.45) and Milbrandt scheme (ME = 0.16 cm) perform the best in simulating the spatial distribution and magnitude of the gauged snow depth, respectively. However, all of these WRF simulations tend to overestimate the snow depth, with ME values of about 0.4 cm. Considering the mean daily T2 in Figure 4, it is found that the spatial distributions of the simulated snow depth are quite similar to those of the mean daily T2. This indicates that the existence of the snow on the ground in the WRF simulations may have led to the underestimation of T2.

In terms of simulating the daily snow depth series during October 4–8, 2018 (Figure 7), the PPSs used in the reference run, except for the CUs (YSU, MSKF, Noah-MP, and Thompson), outperform the PPSs of the same type in capturing the variability of the daily snow depth gauge observations. All of the WRF simulations overestimate the mean snow depth, especially the MYJ scheme, which has mean biases of >0.5 cm. All of the simulations overestimate the snow depth already at the beginning of this snow event (4 October 2018), which is the main reason why the daily snow depth is overestimated in the WRF simulations compared to the gauge observations. This may have been related to the initial conditions of the WRF simulations that the 12 km WRF simulations start to accumulate snow over the TP too early. At the same time, the forcing data for 12 km WRF simulations (i.e., ERA5) overestimates the snow depth over the TP (Orsolini et al., 2019), which may have led to this situation.

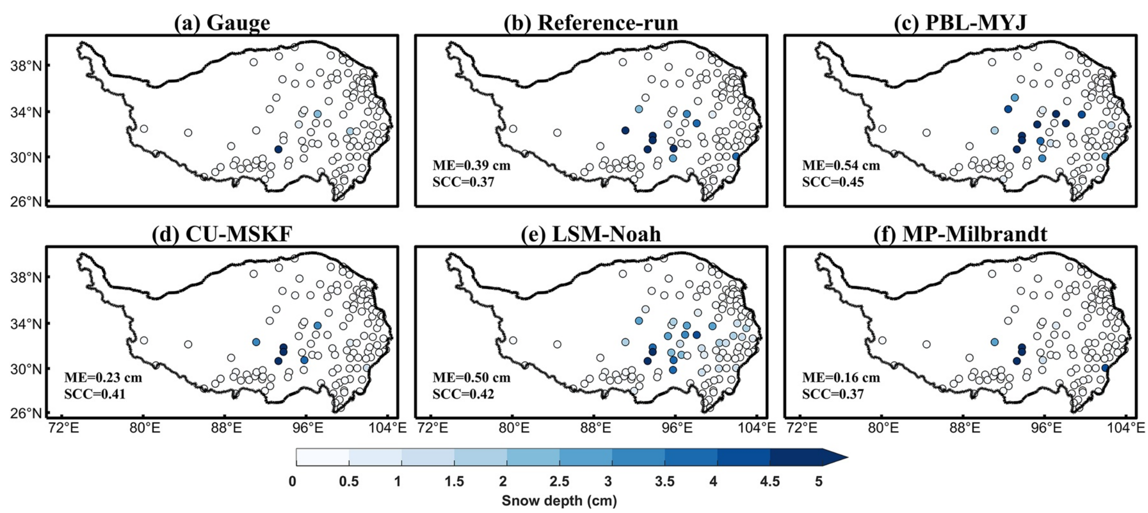


**Figure 6.** Spatial distributions of mean snow depth averaged from October 4 to 8, 2018: (a) gauge observations, and (b–f) WRF simulations over the gauge stations, with ME and SCC calculated based on gauge observations.

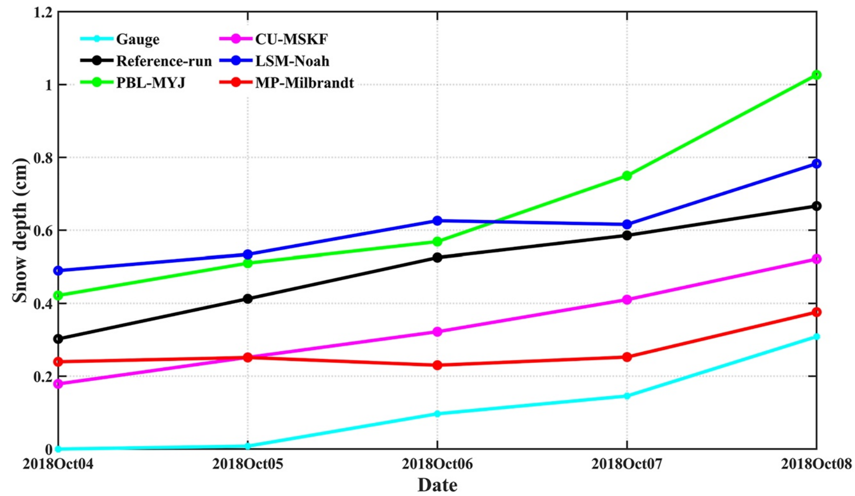


**Figure 7.** Daily snow depth time series for the gauge stations and the WRF simulations during October 4–8, 2018. The values are averaged over 125 stations.

According to the MODIS snow data during the study period, the snow cover extent was the largest on 8 October 2018. Thus, October 8 was selected to evaluate the performance of the WRF in simulating the snow cover. Figure 8 shows the snow cover for the MODIS and WRF simulations on October 8. As expected, the spatial distribution of the snow cover exhibits a pattern similar to that of the snow depth, which is generally captured by all of the WRF simulations, with SCC values of around 0.5. However, it is evident that all of the simulations also overestimate the snow cover extent, which is consistent with the simulated snow depth.

#### 3.3.2. Snowfall Amount

The snowfall amount is one of the most important variables for describing an extreme snow event. Hence, the snowfall amount of the GPM was used as a reference to evaluate the performance of the WRF model in simulating the snowfall amount, which was calculated based on the precipitation and PL. The spatial distributions of the snowfall amount during October 4–8, 2018, for the GPM and WRF simulations are displayed in Figure 9. The most snowfall occurred to the northeast of Nam Co Lake, and the maximum snowfall amount reached 50 mm. However, all of the simulations significantly overestimate the snowfall amount, especially over the southeastern TP. The MRE values of the WRF simulations are greater than 350%. In particular, the MYJ scheme exhibits a considerable difference in simulating the snowfall amount, with an MRE of 745%. The large MRE values of these simulations are partially due to the small snowfall amount over most areas of the TP, and thus, a small bias is sufficient to cause a large MRE value. In terms of simulating the spatial distribution of the snowfall amount, all of the simulations agree well with the GPM, with SCC values of >0.59.

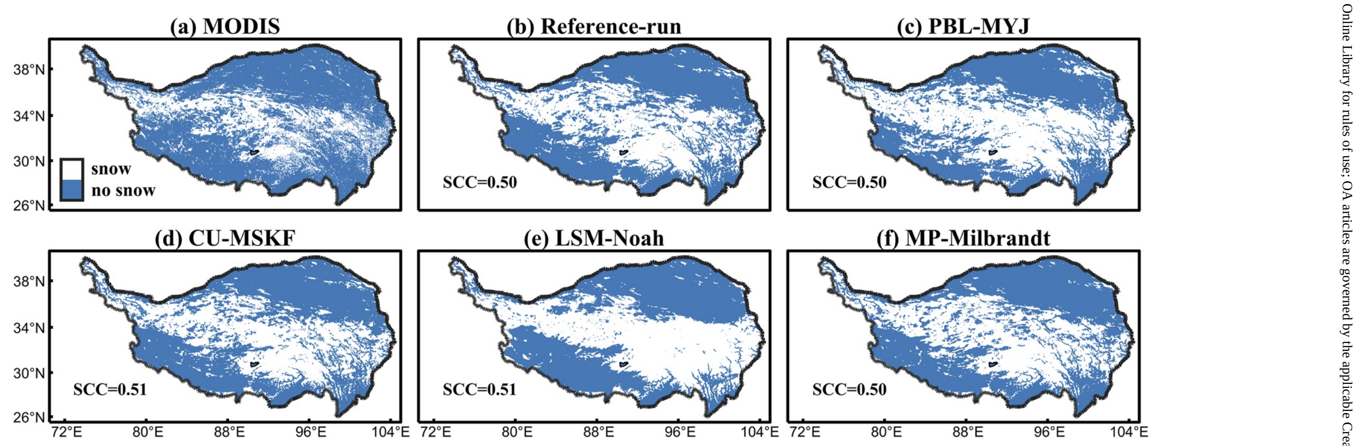


**Figure 8.** Snow cover from (a) MODIS and (b–f) WRF simulations on 8 October 2018, with SCC calculated based on MODIS.

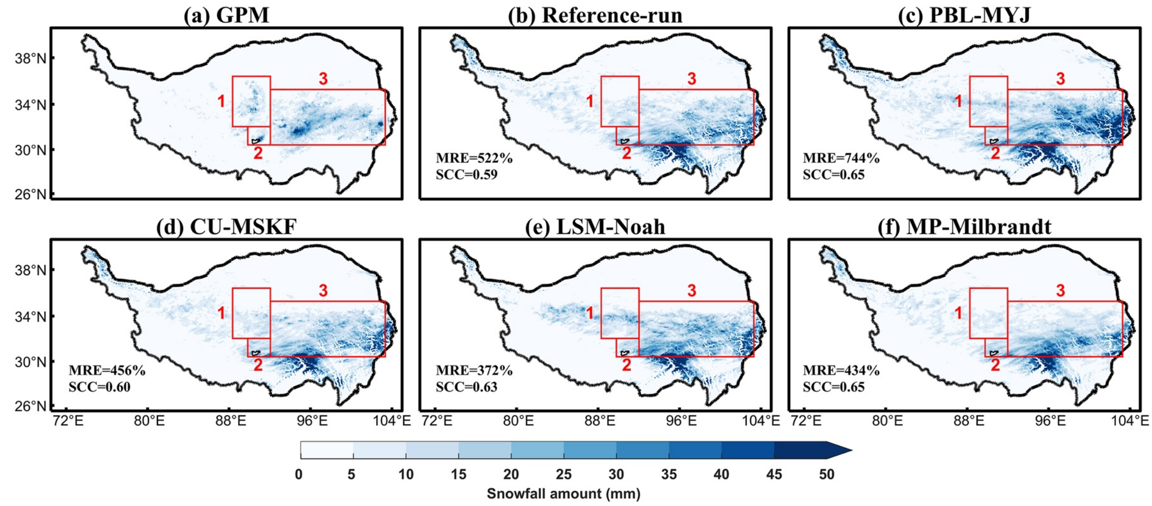


**Figure 9.** Spatial distributions of the snowfall amount during October 4–8, 2018: (a) GPM, and (b–f) WRF simulations, with MRE and SCC calculated based on GPM.

Based on the spatial distributions of the GPM snowfall amount during October 4–8, 2018, three regions were partitioned for further analyses (Figure 9). Specifically, the selection of these three regions should fulfill the following criteria: (a) they cover the areas of snowfall as much as possible; (b) the snowfall in each area is spatially continuous; and (c) they differ as much as possible in terms of magnitude or spatial distribution of snowfall. Eventually, the selected three regions are located in the north (region 1), downwind area (region 2), and east (region 3) of Nam Co Lake. The regional mean accumulated snowfall of the GPM and WRF simulations from October 4 to 8 over the three regions is shown in Figure 10. The accumulated snowfall in region 2 and region 3 is about two to three times that in region 1. The regional mean accumulated snowfall of the GPM in region 1 is about 5 mm and is captured well by all of the simulations. However, the WRF simulations tend to overestimate the accumulated snowfall of the GPM in regions 2 and 3. Specifically, the regional mean accumulated snowfall of the GPM is 7.9 mm in region 2, while the simulated values range from 12 to 15 mm. Moreover, among the simulations, the Noah LSM performs the best in simulating the accumulated snowfall in region 2. The simulated regional mean accumulated snowfall is closer to the GPM in region 3 than in region 2, and the performances of the simulations are quite similar, except for that of the MYJ scheme. These results indicate that the WRF model has a great potential for simulating light snowfall, which is consistent with the conclusion of Liu et al. (2019).

Because the snowfall during October 4–8 in region 2 was typical lake-effect snow, further analysis was conducted. Figure 11 shows that the lake-effect snow event investigated in this study is well visible by the reference data (i.e., snowfall of GPM, and 10 m wind field of ERA5). It can be seen that more intense snowfall occurs over the lake and downwind area. However, there are remarkable differences between all of the simulations and references. None of the WRF simulations capture the characteristics of the lake-effect snow, neither the spatial distribution of

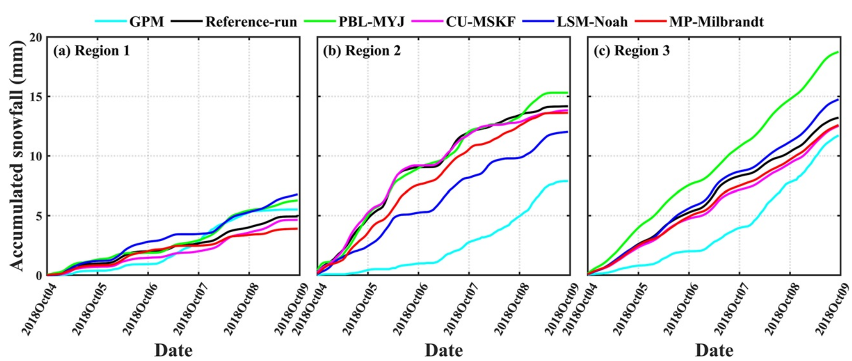


**Figure 10.** Accumulated snowfall from the GPM and WRF simulations from October 4 to 8, 2018. The values are averaged over three regions.

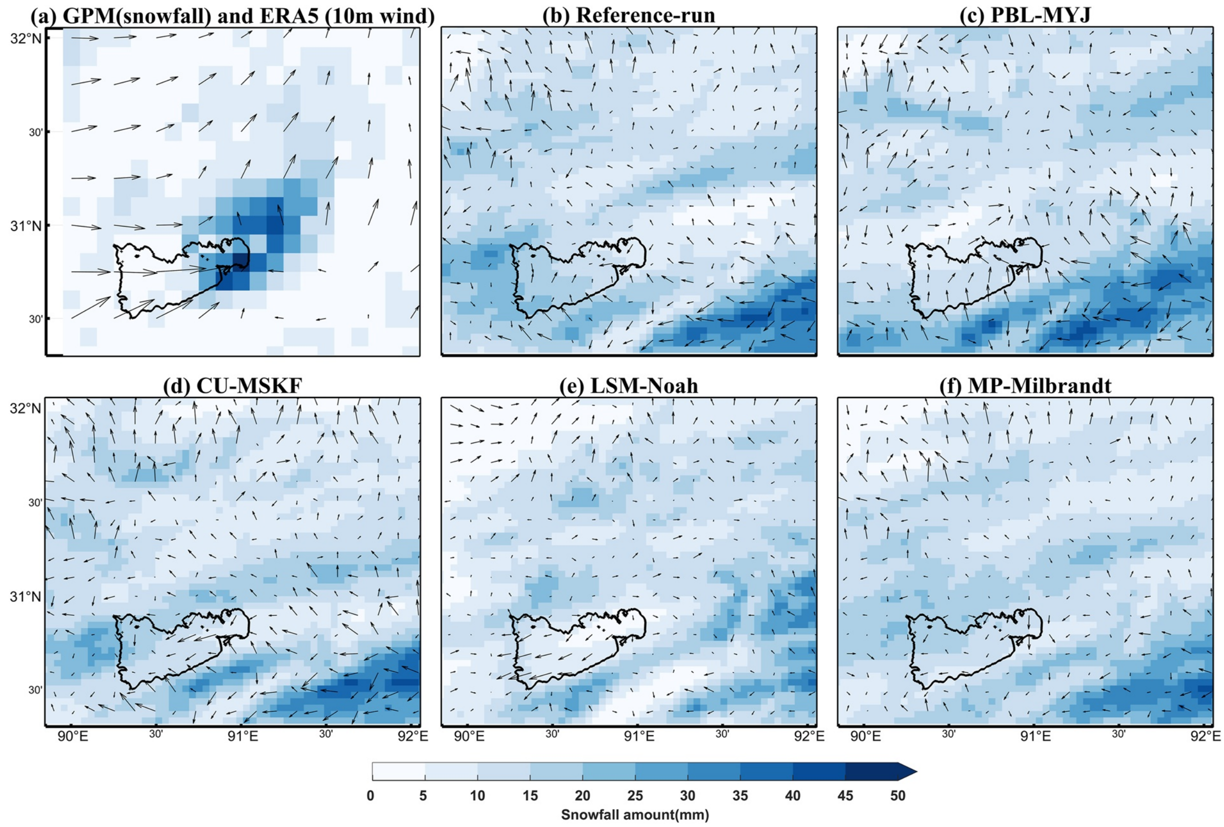


**Figure 11.** Spatial distributions of the snowfall amount and mean 10 m wind from October 4 to 8, 2018, over region 2: (a) GPM and ERA5, and (b–f) WRF simulations.

the snowfall nor the 10 m wind field. To determine why the WRF model fails to accurately simulate the characteristics of lake-effect snow, the mean daily T2 in region 2 was also analyzed. The CMFD accurately depicts the fact that Nam Co Lake acted as a heat source during October 4–8, 2018 (Figure S6 in Supporting Information S1). In fact, all of the WRF simulations also show the lake is a heat source, which is consistent with the CMFD. However, it is found that the simulated temperature of the lake surface and its surroundings all exist large cold biases, which may be one of the primary reasons why all of the WRF simulations fail to reproduce this lake-effect snow event. Moreover, the west wind dominates the wind pattern over the lake in ERA5, while the dominant winds are south or east in the simulations. It can be seen that the airflows over the lake are not accurately captured by the WRF simulations, which is another important reason for the above results.

Although none of the WRF simulations can satisfactorily reproduce the characteristics of the lake-effect snow predicted by theory, that is, the snow mainly falls over the lake and downwind areas, overall, all of the WRF simulations have acceptable performances in simulating the spatial distributions of the snow-related variables over the entire TP. In terms of the performance of the WRF model in simulating the magnitudes of the snow-related variables, the Milbrandt scheme slightly outperforms the other PPSs. The other four PPSs share a similar performance in simulating the snow-related variables.

## 4. Discussion

The performance of the WRF model with different PPSs in simulating snowfall and lake-effect snow (October 4–8, 2018) was investigated over the TP. Generally, all of the simulations capture the main characteristics of the snow-related variables concerning the spatial distributions and magnitudes, which performance are basically consistent with the previous studies (e.g., Liu et al., 2019, 2021, 2022). Meanwhile, due to the limitation of the model and forcing data, possible reasons for these results of snow-related variables can be explained. Therefore, all of the simulations have acceptable performances in simulating both the spatial distributions and magnitudes of the snow-related variables. However, it is difficult to identify the PPS that consistently performs the best. By evaluating the performance of the WRF model in simulating specific weather features at the regional scale, it is found that all of the simulations assessed in this study leave much to be desired. None of these simulations reproduces the spatial distribution features of lake-effect snow most likely due to their inaccurate modeling of the temperature and airflow over the lake surface and its surroundings. This means that the use of optimal PPSs may not be an effective way to improve the accuracy of the WRF model in simulating lake-effect snow events. The sources of these errors may be more related to land surface processes and less associated with atmospheric processes. Coupling with a lake model may be helpful in getting the issue resolved. Previous studies have shown that the typical spatial distribution characteristics of lake-effect snow can be well simulated when the WRF model is coupled with a lake model (Zhao et al., 2022). This is because the lake model can satisfactorily reproduce the variations in the thermal stratification of lake surface temperature by adjusting several key parameters (Wu et al., 2020). As a consequence, simulations of meteorological variables over the lake and surrounding areas can be largely improved (Huang et al., 2019; Wu et al., 2020; Xu et al., 2016). Therefore, a deeper analysis for understanding the mechanisms of lake-effect snow can be conducted by coupling a lake model with the WRF model in the future. Moreover, the effects of the lake model setting on the simulated lake-effect snow are also worth exploring.

Previous studies have shown that snowfall simulations are most sensitive to MPs when the terrain is complex (Liu et al., 2011). In this study, it was found that the Milbrandt scheme performs better than the Thompson scheme in simulating the snow-related variables, while the Thompson scheme has more potential in simulating precipitation over the TP, which has also been reported in other studies (Li et al., 2017; Maussion et al., 2014). Although the cloud structures and precipitation mechanisms simulated using the Thompson and Mlibrandt schemes are consistent (Milbrandt et al., 2012; Zha et al., 2020), the consideration of the physical processes in the Milbrandt scheme is more comprehensive. In particular, the main conversion terms of the snow in the Milbrandt scheme are more variable and realistic than those in the Thompson scheme (Mei et al., 2015), leading to reliable simulations of the snow-related variables (Milbrandt et al., 2012).

In addition, the Noah LSM exhibits a slightly better performance than the Noah-MP in simulating snowfall, but this is not the case for simulating snow depth. The Noah LSM simply assumes that snowfall occurs when the surface air temperature is lower than the freezing point, while the Noah-MP LSM applies a relatively complex function to simulate the snowfall (Liu et al., 2019). In fact, the surface air temperature at the location of the snowfall during this event is lower than the freezing point most of the time, thus the Noah LSM tends to exhibit better performance in simulating snowfall than the Noah-MP LSM. For the simulations of the snow depth, the Noah LSM has a deficiency in simulating the albedo over snow-covered areas (Meng et al., 2018). Specifically, the Noah LSM only considers a single layer of snowpack, and thus, it tends to overestimate the snow albedo needed to maintain the snow on the ground (Chen et al., 2014), resulting in a cold bias and overestimation of the snow depth over the TP. Hence, when conducting the WRF simulations of snow events, the albedo parameterization can be switched off and replaced with the MODIS albedo (Wang et al., 2021). In addition, the improved snow albedo parameterization scheme developed by Liu et al. (2021, 2022) has a strong potential for snow event simulation over the TP. This also provides a great option for future modeling to obtain more reliable simulations of snow-related variables.

The results of this study may include multiple sources of uncertainty related to the data availability and model simulations. On the one hand, the gauge stations are sparsely and unevenly distributed over the western TP. Although satellite-based or station-based gridded observations were also used for the evaluation, there are differences between these two types of observations. For example, the GPM and CMFD exhibit dry and cold biases, respectively, when compared with the gauge observations. On the other hand, the distance between the actual locations of the gauges and the associated grid point may lead to large elevation differences in the complex terrain (Lin et al., 2021; Wang et al., 2021). Thus, the point to point comparisons between the observations and simulations may have discrepancies. In addition, all of the WRF simulations with different PPSs assessed in this study exhibit cold biases. The cold bias may be affected by the references used. For example, in-situ observations are generally located in valleys (Li, 2018) that have relatively higher temperatures than their surroundings. Large deviations exist in the derived temperature data sets as shown by Prein et al. (2022). Besides, the forcing data (i.e., ERA5) largely overestimates the snow depth over the TP (Orsolini et al., 2019), which may also contribute to the cold bias in the WRF simulations. Although it has been found that bias correction of the ERA5 initial snow depth can significantly reduce cold biases when conducting the WRF simulations (Lin et al., 2021; Wang et al., 2021), the cold bias over the TP could not be eliminated. As was previously mentioned, these cold biases may be caused by the systematic cold bias of the WRF model when conducting simulations over high altitude regions (Bonekamp et al., 2018; Gao et al., 2015). Therefore, it is necessary to further investigate whether there are similar situations when using other regional climate models to conduct convection-permitting simulations over the TP. At last, it is needed to emphasize that the results of this study are valid for the particular case and some of the details on how certain model physics perform may be case-dependent. Future studies should focus on other cases and longer time periods.

## 5. Summary and Conclusions

In this study, the performance of the WRF model with different PPSs in simulating snowfall and lake-effect snow (October 4–8, 2018) over the TP was investigated. Various parameterization schemes were applied in the WRF model, including two PBLs (YSU and MYJ), two CUs (no cumulus and MSKF), two LSMs (Noah and Noah-MP), and two MPs (Thompson and Milbrandt), and the results were compared. The following conclusions were drawn.

1. All of the WRF simulations agree well with the observations in simulating the mean daily precipitation over the TP, even though they tend to exhibit wet biases. Generally, the YSU scheme, MSKF scheme, Noah LSM, and Thompson scheme are the best schemes (SCCs = 0.56–0.71; mean MREs = 27.7%–53.6%) for simulating the mean daily precipitation during this snow event, compared with the gauge observations. The results are similar when compared with the satellite observations (i.e., GPM). For the simulation of the accumulated precipitation during this event, the above-mentioned PPSs also perform better than the others.
2. All of the WRF simulations with different PPSs perform reasonably well in simulating the spatial distribution of the mean daily T2. When compared with the gauge observations and CMFD, their SCC values are >0.86. However, cold biases exist for all of the PPSs, with mean ME values ranging from −3.3° to −2.9°C (−1.7° to −1.2°C) when compared with the gauge observations (CMFD). In addition, all of the WRF PPSs perform excellently in simulating the variability of the hourly T2, even though the cold biases are up to 3°C over the TP when compared with the gauge observations.
3. All of the PPSs assessed exhibit acceptable performances in simulating the spatial distributions of the snow depth, snow cover, and snowfall amount, with SCC values between simulations and observations of greater than 0.37, 0.50, and 0.59, respectively. However, all of the WRF simulations overestimate the snow depth of gauge observations and snowfall amount of the GPM during October 4–8, 2018. Overall, the Milbrandt scheme slightly outperforms the other PPSs in simulating the magnitudes of the snow-related variables. However, none of them can satisfactorily reproduce the characteristics of this lake-effect snow event; that is, more snow occurs over the lake and downwind areas, due to their inaccurate modeling of the temperature and airflow over the lake surface and its surroundings.

## Data Availability Statement

The GPM data is available at the NASA Goddard Earth Sciences Data and Information Services Center (https://pmm.nasa.gov/data-access/downloads/gpm). The TP boundary data and CMFD are available at National Tibetan Plateau Data Center (http://data.tpdc.ac.cn).

**Acknowledgments**
This work was partially supported by the National Natural Science Foundation of China (Grant 52079093), the Hubei Provincial Natural Science Foundation of China (Grant 2020CFA100), and the Overseas Expertise Introduction Project for Discipline Innovation (111 Project) funded by the Ministry of Education and State Administration of Foreign Experts Affairs P.R. China (Grant B18037). This is a contribution to the Swedish national strategic research program MERGE and no 15 to CORDEX-FPS-CPTP.

## References

Argent, R., Sun, X., Semazzi, F., Xie, L., & Liu, B. (2015). The development of a customization framework for the WRF model over the Lake Victoria Basin, Eastern Africa on seasonal timescales. *Advances in Meteorology*, *2015*, 1–15. https://doi.org/10.1155/2015/653473
Behrangi, A., Tian, Y. D., Lambrigtsen, B. H., & Stephens, G. L. (2014). What does CloudSat reveal about global land precipitation detection by other spaceborne sensors? *Water Resources Research*, *50*(6), 4893–4905. https://doi.org/10.1002/2013wr014566
Beljaars, A. C. M., Brown, A. R., & Wood, N. (2004). A new parametrization of turbulent orographic form drag. *Quarterly Journal of the Royal Meteorological Society*, *130*(599), 1327–1347. https://doi.org/10.1256/qj.03.73
Bonan, G. B. (1995). Sensitivity of a GCM simulation to inclusion of inland water surfaces. *Journal of Climate*, *8*(11), 2691–2704. https://doi.org/10.1175/1520-0442(1995)008<2691:soagst>2.0.co;2
Bonekamp, P. N. J., Collier, E., & Immerzeel, W. W. (2018). The impact of spatial resolution, land use, and spinup time on resolving spatial precipitation patterns in the Himalayas. *Journal of Hydrometeorology*, *19*(10), 1565–1581. https://doi.org/10.1175/jhm-d-17-0212.1
Chen, F., Barlage, M., Tewari, M., Rasmussen, R., Jin, J. M., Lettenmaier, D., et al. (2014). Modeling seasonal snowpack evolution in the complex terrain and forested Colorado headwaters region: A model intercomparison study. *Journal of Geophysical Research: Atmospheres*, *119*(24), 13795–13819. https://doi.org/10.1002/2014jd022167

Copernicus Climate Change Service (C3S). (2017). ERA5: Fifth generation of ECMWF atmospheric reanalyses of the global climate. Copernicus Climate Change Service Climate Data Store (CDS). Retrieved from https://cds.climate.copernicus.eu/cdsapp#!/home

Dai, Y. F., Chen, D. L., Yao, T. D., & Wang, L. (2020). Large lakes over the Tibetan Plateau may boost snow downwind: Implications for snow disaster. *Science Bulletin*, *65*(20), 1713–1717. https://doi.org/10.1016/j.scib.2020.06.012

Dai, Y. F., Wang, L., Yao, T. D., Li, X. Y., Zhu, L. J., & Zhang, X. W. (2018). Observed and simulated lake effect precipitation over the Tibetan Plateau: An initial study at Nam Co Lake. *Journal of Geophysical Research: Atmospheres*, *123*(13), 6746–6759. https://doi.org/10.1029/2018jd028330

Dai, Y. F., Yao, T. D., Wang, L., Li, X. Y., & Zhang, X. W. (2020). Contrasting roles of a Large Alpine Lake on Tibetan Plateau in shaping regional precipitation during summer and autumn. *Frontiers in Earth Science*, *8*, 358. https://doi.org/10.3389/feart.2020.00358

Dong, S. Y., Peng, F., You, Q. G., Guo, J., & Xue, X. (2018). Lake dynamics and its relationship to climate change on the Tibetan Plateau over the last four decades. *Regional Environmental Change*, *18*(2), 477–487. https://doi.org/10.1007/s10113-017-1211-8

Eichenlaub, V. L. (1970). Lake effect snowfall to the lee of the Great Lakes: Its role in Michigan. *Bulletin of the American Meteorological Society*, *51*(5), 403–413. https://doi.org/10.1175/1520-0477(1970)051<0403:lesttl>2.0.co;2

Gao, Y. H., Xu, J. W., & Chen, D. L. (2015). Evaluation of WRF mesoscale climate simulations over the Tibetan Plateau during 1979–2011. *Journal of Climate*, *28*(7), 2823–2841. https://doi.org/10.1175/jcli-d-14-00300.1

Hao, X. H. (2021). *A new MODIS snow cover extent product over China (2000-2020)*. National Tibetan Plateau Data Center. https://doi.org/10.11888/Snow.tpdc.271387

Hao, X. H., Huang, G. H., Zheng, Z. J., Sun, X. L., Ji, W. Z., Zhao, H. Y., et al. (2022). Development and validation of a new MODIS snow-cover-extent product over China. *Hydrology and Earth System Sciences*, *26*(8), 1937–1952. https://doi.org/10.5194/hess-26-1937-2022

He, J., Yang, K., Tang, W. J., Lu, H., Qin, J., Chen, Y. Y., & Li, X. (2020). The first high-resolution meteorological forcing dataset for land process studies over China. *Scientific Data*, *7*(1), 25. https://doi.org/10.1038/s41597-020-0369-y

Henderson, G. R., Peings, Y., Furtado, J. C., & Kushner, P. J. (2018). Snow-atmosphere coupling in the Northern Hemisphere. *Nature Climate Change*, *8*(11), 954–963. https://doi.org/10.1038/s41558-018-0295-6

Hong, S. Y., Noh, Y., & Dudhia, J. (2006). A new vertical diffusion package with an explicit treatment of entrainment processes. *Monthly Weather Review*, *134*(9), 2318–2341. https://doi.org/10.1175/mwr3199.1

Huang, A. N., Wang, J. B., Dai, Y. J., Yang, K., Wei, N., Wu, Y., et al. (2019). Evaluating and improving the performance of three 1-D lake models in a Large Deep Lake of the Central Tibetan Plateau. *Journal of Geophysical Research: Atmospheres*, *124*(6), 3143–3167. https://doi.org/10.1029/2018jd029610

Huffman, G. J., Stocker, E. F., Bolvin, D. T., Nelkin, E. J., & Jackson, T. (2019). *GPM IMERG final precipitation L3 half hourly 0.1 degree x 0.1 degree V06, Greenbelt, MD*. Goddard Earth Sciences Data and Information Services Center (GES DISC). https://doi.org/10.5067/GPM/IMERG/3B-HH/06

Iacono, M. J., Delamere, J. S., Mlawer, E. J., Shephard, M. W., Clough, S. A., & Collins, W. D. (2008). Radiative forcing by long-lived greenhouse gases: Calculations with the AER radiative transfer models. *Journal of Geophysical Research*, *113*(D13), D13103. https://doi.org/10.1029/2008jd009944

Immerzeel, W. W., Wanders, N., Lutz, A. F., Shea, J. M., & Bierkens, M. F. P. (2015). Reconciling high-altitude precipitation in the Upper Indus Basin with glacier mass balances and runoff. *Hydrology and Earth System Sciences*, *19*(11), 4673–4687. https://doi.org/10.5194/hess-19-4673-2015

Janjic, Z. I. (1994). The Step-Mountain Eta coordinate Model: Further developments of the convection, viscous sublayer, and turbulence closure schemes. *Monthly Weather Review*, *122*(5), 927–945. https://doi.org/10.1175/1520-0493(1994)122<0927:tsmecm>2.0.co;2

Kristovich, D. A. R., Laird, N. F., & Hjelmfelt, M. R. (2003). Convective evolution across Lake Michigan during a widespread lake-effect snow event. *Monthly Weather Review*, *131*(4), 643–655. https://doi.org/10.1175/1520-0493(2003)131<0643:cealmd>2.0.co;2

Lavoie, R. L. (1972). A mesoscale numerical model of lake-effect storms. *Journal of the Atmospheric Sciences*, *29*(6), 1025–1040. https://doi.org/10.1175/1520-0469(1972)029<1025:amnmol>2.0.co;2

Li, D. H., Qi, Y. C., & Chen, D. L. (2022). Changes in rain and snow over the Tibetan Plateau based on IMERG and Ground-based observation. *Journal of Hydrology*, *606*, 127400. https://doi.org/10.1016/j.jhydrol.2021.127400

Li, J. (2018). Hourly station-based precipitation characteristics over the Tibetan Plateau. *International Journal of Climatology*, *38*(3), 1560–1570. https://doi.org/10.1002/joc.5281

Li, L., Gochis, D. J., Sobolowski, S., & Mesquita, M. D. S. (2017). Evaluating the present annual water budget of a Himalayan headwater river basin using a high-resolution atmosphere-hydrology model. *Journal of Geophysical Research: Atmospheres*, *122*(9), 4786–4807. https://doi.org/10.1002/2016jd026279

Li, M., Ma, Y., Hu, Z., Ishikawa, H., & Oku, Y. (2009). Snow distribution over the Namco lake area of the Tibetan Plateau. *Hydrology and Earth System Sciences*, *13*(11), 2023–2030. https://doi.org/10.5194/hess-13-2023-2009

Li, Y. Z., Qin, X., Liu, Y. S., Jin, Z. Z., Liu, J., Wang, L. H., & Chen, J. Z. (2022). Evaluation of long-term and high-resolution gridded precipitation and temperature products in the Qilian Mountains, Qinghai-Tibet Plateau. *Frontiers in Environmental Science*, *10*, 906821. https://doi.org/10.3389/fenvs.2022.906821

Lin, Q., Chen, J., Chen, D. L., Wang, X., Li, W., & Scherer, D. (2021). Impacts of bias-corrected ERA5 initial snow depth on dynamical downscaling simulations for the Tibetan Plateau. *Journal of Geophysical Research: Atmospheres*, *126*(23), e2021JD035625. https://doi.org/10.1029/2021jd035625

Liu, C. H., Ikeda, K., Rasmussen, R., Barlage, M., Newman, A. J., Prein, A. F., et al. (2017). Continental-scale convection-permitting modeling of the current and future climate of North America. *Climate Dynamics*, *49*(1–2), 71–95. https://doi.org/10.1007/s00382-016-3327-9

Liu, C. H., Ikeda, K., Thompson, G., Rasmussen, R., & Dudhia, J. (2011). High-resolution simulations of wintertime precipitation in the Colorado headwaters region: Sensitivity to physics parameterizations. *Monthly Weather Review*, *139*(11), 3533–3553. https://doi.org/10.1175/mwr-d-11-00009.1

Liu, L., Ma, Y. M., Menenti, M., Su, R. M. Z., Yao, N., & Ma, W. Q. (2021). Improved parameterization of snow albedo in Noah coupled with weather research and forecasting: Applicability to snow estimates for the Tibetan Plateau. *Hydrology and Earth System Sciences*, *25*(9), 4967–4981. https://doi.org/10.5194/hess-25-4967-2021

Liu, L., Ma, Y. M., Menenti, M., Zhang, X. Z., & Ma, W. Q. (2019). Evaluation of WRF modeling in relation to different land surface schemes and initial and boundary conditions: A snow event simulation over the Tibetan Plateau. *Journal of Geophysical Research: Atmospheres*, *124*(1), 209–226. https://doi.org/10.1029/2018jd029208

Liu, L., Menenti, M., Ma, Y. M., & Ma, W. Q. (2022). Improved parameterization of snow albedo in WRF plus Noah: Methodology based on a severe snow event on the Tibetan Plateau. *Advances in Atmospheric Sciences*, *39*(7), 1079–1102. https://doi.org/10.1007/s00376-022-1232-1

Ma, Y., Wang, Y., Wu, R., Hu, Z., Yang, K., Li, M., et al. (2009). Recent advances on the study of atmosphere-land interaction observations on the Tibetan Plateau. *Hydrology and Earth System Sciences*, *13*(7), 1103–1111. https://doi.org/10.5194/hess-13-1103-2009

Maussion, F., Scherer, D., Molg, T., Collier, E., Curio, J., & Finkelnburg, R. (2014). Precipitation seasonality and variability over the Tibetan Plateau as resolved by the high Asia reanalysis. *Journal of Climate*, *27*(5), 1910–1927. https://doi.org/10.1175/jcli-d-13-00282.1

Mei, H., Shen, X., Wang, W., & Huang, W. (2015). Evaluation and comparison of two double-moment bulk microphysics schemes using WRF single-column model. *Plateau Meteorology*, *34*(4), 890–909.

Meng, X., Lyu, S., Zhang, T., Zhao, L., Li, Z., Han, B., et al. (2018). Simulated cold bias being improved by using MODIS time-varying albedo in the Tibetan Plateau in WRF model. *Environmental Research Letters*, *13*(4), 044028. https://doi.org/10.1088/1748-9326/aab44a

Milbrandt, J. A., Glazer, A., & Jacob, D. (2012). Predicting the snow-to-liquid ratio of surface precipitation using a bulk microphysics scheme. *Monthly Weather Review*, *140*(8), 2461–2476. https://doi.org/10.1175/mwr-d-11-00286.1

Milbrandt, J. A., & Yau, M. K. (2005a). A multimoment bulk microphysics parameterization. Part I: Analysis of the role of the spectral shape parameter. *Journal of the Atmospheric Sciences*, *62*(9), 3051–3064. https://doi.org/10.1175/jas3534.1

Milbrandt, J. A., & Yau, M. K. (2005b). A multimoment bulk microphysics parameterization. Part II: A proposed three-moment closure and scheme description. *Journal of the Atmospheric Sciences*, *62*(9), 3065–3081. https://doi.org/10.1175/jas3535.1

Niu, G. Y., Yang, Z. L., Mitchell, K. E., Chen, F., Ek, M. B., Barlage, M., et al. (2011). The community Noah land surface model with multiparameterization options (Noah-MP): 1. Model description and evaluation with local-scale measurements. *Journal of Geophysical Research*, *116*(D12), D12109. https://doi.org/10.1029/2010jd015139

Notaro, M., Holman, K., Zarrin, A., Fluck, E., Vavrus, S., & Bennington, V. (2013). Influence of the Laurentian Great Lakes on regional climate. *Journal of Climate*, *26*(3), 789–804. https://doi.org/10.1175/jcli-d-12-00140.1

Notaro, M., Zarrin, A., Vavrus, S., & Bennington, V. (2013). Simulation of heavy lake-effect snowstorms across the Great Lakes Basin by RegCM4: Synoptic climatology and variability. *Monthly Weather Review*, *141*(6), 1990–2014. https://doi.org/10.1175/mwr-d-11-00369.1

Orsolini, Y., Wegmann, M., Dutra, E., Liu, B. Q., Balsamo, G., Yang, K., et al. (2019). Evaluation of snow depth and snow cover over the Tibetan Plateau in global reanalyses using in situ and satellite remote sensing observations. *The Cryosphere*, *13*(8), 2221–2239. https://doi.org/10.5194/tc-13-2221-2019

Ou, T. H., Chen, D. L., Chen, X. C., Lin, C. G., Yang, K., Lai, H. W., & Zhang, F. Q. (2020). Simulation of summer precipitation diurnal cycles over the Tibetan Plateau at the gray-zone grid spacing for cumulus parameterization. *Climate Dynamics*, *54*(7–8), 3525–3539. https://doi.org/10.1007/s00382-020-05181-x

Powers, J. G., Klemp, J. B., Skamarock, W. C., Davis, C. A., Dudhia, J., Gill, D. O., et al. (2017). The weather research and forecasting model: Overview, system efforts, and future directions. *Bulletin of the American Meteorological Society*, *98*(8), 1717–1737. https://doi.org/10.1175/bams-d-15-00308.1

Prein, A. F., Ban, N., Ou, T., Tang, J., Sakaguchi, K., Collier, E., et al. (2022). Towards ensemble-based kilometer-scale climate simulations over the third pole region. *Climate Dynamics*, *60*(11–12), 4055–4081. https://doi.org/10.1007/s00382-022-06543-3

Ren, L. Y., Duan, K. Q., & Xin, R. (2020). Impact of future loss of glaciers on precipitation pattern: A case study from south-eastern Tibetan Plateau. *Atmospheric Research*, *242*, 104984. https://doi.org/10.1016/j.atmosres.2020.104984

Scott, R. W., & Huff, F. A. (1996). Impacts of the Great Lakes on regional climate conditions. *Journal of Great Lakes Research*, *22*(4), 845–863. https://doi.org/10.1016/s0380-1330(96)71006-7

Shen, S. S. P., Yao, R. Z., Ngo, J., Basist, A. M., Thomas, N., & Yao, T. D. (2015). Characteristics of the Tibetan Plateau snow cover variations based on daily data during 1997-2011. *Theoretical and Applied Climatology*, *120*(3–4), 445–453. https://doi.org/10.1007/s00704-014-1185-0

Sims, E. M., & Liu, G. S. (2015). A parameterization of the probability of snow-rain transition. *Journal of Hydrometeorology*, *16*(4), 1466–1477. https://doi.org/10.1175/jhm-d-14-0211.1

Skamarock, W. C., & Klemp, J. B. (2008). A time-split nonhydrostatic atmospheric model for weather research and forecasting applications. *Journal of Computational Physics*, *227*(7), 3465–3485. https://doi.org/10.1016/j.jcp.2007.01.037

Su, D. S., Wen, L. J., Gao, X. Q., Lepparanta, M., Song, X. Y., Shi, Q. Q., & Kirillin, G. (2020). Effects of the largest lake of the Tibetan Plateau on the regional climate. *Journal of Geophysical Research: Atmospheres*, *125*(22), e2020JD033396. https://doi.org/10.1029/2020jd033396

Subin, Z. M., Riley, W. J., & Mironov, D. (2012). An improved lake model for climate simulations: Model structure, evaluation, and sensitivity analyses in CESM1. *Journal of Advances in Modeling Earth Systems*, *4*(1), M02001. https://doi.org/10.1029/2011ms000072

Tewari, M., Chen, F., Wang, W., Dudhia, J., LeMone, M. A., Mitchell, K., et al. (2004). Implementation and verification of the unified NOAH land surface model in the WRF model. In *20th conference on weather analysis and forecasting/16th conference on numerical weather prediction* (Vol. 1115). American Meteorological Society.

Thompson, G., Field, P. R., Rasmussen, R. M., & Hall, W. D. (2008). Explicit forecasts of winter precipitation using an improved bulk microphysics scheme. Part II: Implementation of a New snow parameterization. *Monthly Weather Review*, *136*(12), 5095–5115. https://doi.org/10.1175/2008mwr2387.1

Vavrus, S., Notaro, M., & Zarrin, A. (2013). The role of ice cover in heavy lake-effect snowstorms over the Great Lakes Basin as simulated by RegCM4. *Monthly Weather Review*, *141*(1), 148–165. https://doi.org/10.1175/mwr-d-12-00107.1

Wang, X., Tolksdorf, V., Otto, M., & Scherer, D. (2021). WRF-based dynamical downscaling of ERA5 reanalysis data for High Mountain Asia: Towards a new version of the high Asia refined analysis. *International Journal of Climatology*, *41*(1), 743–762. https://doi.org/10.1002/joc.6686

Wen, L. J., Nagabhatla, N., Zhao, L., Li, Z. G., & Chen, S. Q. (2015). Impacts of salinity parameterizations on temperature simulation over and in a hypersaline lake. *Chinese Journal of Oceanology and Limnology*, *33*(3), 790–801. https://doi.org/10.1007/s00343-015-4153-3

Williams, K., Chamberlain, J., Buontempo, C., & Bain, C. (2015). Regional climate model performance in the Lake Victoria Basin. *Climate Dynamics*, *44*(5–6), 1699–1713. https://doi.org/10.1007/s00382-014-2201-x

Wu, Y., Huang, A. N. L., Yang, X. Y., Qiu, B., Wen, L. J., Zhang, Z., et al. (2020). Improvements of the coupled WRF-Lake model over Lake Nam Co, Central Tibetan Plateau. *Climate Dynamics*, *55*(9–10), 2703–2724. https://doi.org/10.1007/s00382-020-05402-3

Wu, Y., Huang, A. N., Yang, B., Dong, G. T., Wen, L. J., Lazhu, et al. (2019). Numerical study on the climatic effect of the lake clusters over Tibetan Plateau in summer. *Climate Dynamics*, *53*(9–10), 5215–5236. https://doi.org/10.1007/s00382-019-04856-4

Xiao, Z. X., & Duan, A. M. (2016). Impacts of Tibetan Plateau snow cover on the interannual variability of the East Asian Summer Monsoon. *Journal of Climate*, *29*(23), 8495–8514. https://doi.org/10.1175/jcli-d-16-0029.1

Xie, Z. P., Hu, Z. Y., Gu, L. L., Sun, G. H., Du, Y. Z., & Yan, X. Q. (2017). Meteorological forcing datasets for blowing snow modeling on the Tibetan Plateau: Evaluation and intercomparison. *Journal of Hydrometeorology*, *18*(10), 2761–2780. https://doi.org/10.1175/jhm-d-17-0075.1

Xu, L. J., Liu, H. Z., Du, Q., & Wang, L. (2016). Evaluation of the WRF-lake model over a highland freshwater lake in southwest China. *Journal of Geophysical Research: Atmospheres*, *121*(23), 13989–14005. https://doi.org/10.1002/2016jd025396

10.1029/2022JD038433


Yang, J. X., Huang, M. T., & Zhai, P. M. (2021). Performance of the CRA-40/land, CMFD, and ERA-interim datasets in reflecting changes in surface air temperature over the Tibetan Plateau. *Journal of Meteorological Research*, *35*(4), 663–672. https://doi.org/10.1007/s13351-021-0196-x

Yang, K., & He, J. (2019). *China meteorological forcing dataset (1979-2018)*. National Tibetan Plateau Data Center. https://doi.org/10.11888/AtmosphericPhysics.tpe.249369.file

Yao, T. D., Bolch, T., Chen, D. L., Gao, J., Immerzeel, W., Piao, S., et al. (2022). The imbalance of the Asian water tower. *Nature Reviews Earth & Environment*, *3*(10), 618–632. https://doi.org/10.1038/s43017-022-00299-4

Zha, S. J., Zhang, H. J., Li, X. X., Hua, S. F., & Chen, B. J. (2020). Numerical simulation of precipitation processes during the opening ceremony of the Nanjing 2014 Youth Olympic Games. *Chinese Journal of Atmospheric Sciences*, *44*(6), 1258–1274.

Zhang, G. Q., Yao, T. D., Piao, S. L., Bolch, T., Xie, H. J., Chen, D. L., et al. (2017). Extensive and drastically different Alpine Lake changes on Asia's high plateaus during the past four decades. *Geophysical Research Letters*, *44*(1), 252–260. https://doi.org/10.1002/2016gl072033

Zhang, G. Q., Yao, T. D., Xie, H. J., Yang, K., Zhu, L. P., Shum, C. K., et al. (2020). Response of Tibetan Plateau lakes to climate change: Trends, patterns, and mechanisms. *Earth-Science Reviews*, *208*, 103269. https://doi.org/10.1016/j.earscirev.2020.103269

Zhao, Z. Z., Huang, A. N., Ma, W. Q., Wu, Y., Wen, L. J., Lazhu, & Gu, C. L. (2022). Effects of Lake Nam Co and surrounding terrain on extreme precipitation over Nam Co Basin, Tibetan Plateau: A case study. *Journal of Geophysical Research: Atmospheres*, *127*(10), e2021JD036190. https://doi.org/10.1029/2021jd036190

Zheng, Y., Alapaty, K., Herwehe, J. A., Del Genio, A. D., & Niyogi, D. (2016). Improving high-resolution weather forecasts using the Weather Research and Forecasting (WRF) model with an updated Kain-Fritsch scheme. *Monthly Weather Review*, *144*(3), 833–860. https://doi.org/10.1175/mwr-d-15-0005.1

Zhou, X., Yang, K., Beljaars, A., Li, H. D., Lin, C. G., Huang, B., & Wang, Y. (2019). Dynamical impact of parameterized turbulent orographic form drag on the simulation of winter precipitation over the western Tibetan Plateau. *Climate Dynamics*, *53*(1–2), 707–720. https://doi.org/10.1007/s00382-019-04628-0

Zhou, X., Yang, K., & Wang, Y. (2018). Implementation of a turbulent orographic form drag scheme in WRF and its application to the Tibetan Plateau. *Climate Dynamics*, *50*(7–8), 2443–2455. https://doi.org/10.1007/s00382-017-3677-y